Theoretical and Experimental Study of the Rovibrational Spectrum of He_2-CO[†]

Xiao-Gang Wang and Tucker Carrington, Jr.*[,†]

Chemistry Department, Queen's University, Kingston, Ontario K7L 3N6, Canada

A. R. W. McKellar[‡]

Steacie Institute for Molecular Sciences, National Research Council of Canada, Ottawa, Ontario K1A 0R6, Canada

Received: May 21, 2009; Revised Manuscript Received: August 25, 2009

We report calculated microwave and infrared ro-vibrational transitions of the van der Waals complex He_2-CO. The calculations were done using a product basis and a Lanczos eigensolver, together with He−CO and He−He potential functions taken from the literature. The results are found to be in good agreement with previously reported experimental results, and they enable the experimental assignments to be clarified, augmented, and (in one case) corrected. Unlike some other van der Waals complexes with two He atoms such as He_2-N_2O, it is not possible to associate a set of energy levels with the "torsional" motion of the two He atoms on a ring encircling the dopant (in this case CO). Although we assume that the dipole moment is along the CO axis we find nonetheless that many transitions have appreciable intensity due to ro-vibrational coupling.

I. Introduction

In recent years, infrared and microwave spectra of several small molecules embedded in helium clusters have been observed and calculated.[1−8] From such spectra one can extract information about the intermolecular interactions that hold the clusters together, and about the cluster structure and dynamics, including helium superfluid effects. Given a reliable potential energy surface for the helium−dopant molecule system, it is possible to compute accurate energy levels and spectra for smaller clusters of this type with one, two, or (possibly) three He atoms, as shown for example by our recent calculations for He_2-N_2O,[6] $-CO_2$,[9] and −OCS.[10] For larger helium clusters such calculations are not practical, and it is necessary to use quantum Monte Carlo type simulations.[11−15] It is important to assess the reliability of these statistical simulation techniques by testing them against more exact eigensolver techniques in the cluster size range where the applicability of the two methods overlap, that is, clusters with two or three He atoms.

In this paper we present results of calculations on He_2-CO and use the results to assign a number of new and previously reported microwave and infrared transitions. We find that the rotation-vibration energy level pattern of He_2-CO is rather different from those of previously studied systems like He_2-N_2O[6] or He_2-Cl_2,[16] and more difficult to understand on the basis of simple models. A He_N-CO cluster has $(N + 1)$ stretch coordinates and $(2N - 1)$ bend coordinates, together with three Euler angles describing its orientation in space. If the CO distance is fixed (for example at the known value for the ground state of the monomer), the number of stretch coordinates is reduced to N. For $N = 2$, it is possible, even using a simple product basis, to compute ro-vibrational levels using modern iterative methods, though the basis sets are large. To do so, one uses Gauss quadrature and evaluates matrix−vector products sequentially.[17−24] This approach can be used to compute the spectrum of any molecule with four or fewer atoms, but it is especially useful for helium−dopant clusters because in this case the required total potential energy function can be obtained (to a good approximation) as a sum of the He−dopant and He−He potentials. Even for $N = 3$, it should now be possible to obtain energy levels and spectra using an iterative eigensolver in conjunction with contracted basis functions, though this has not yet been demonstrated.[24,25]

There have been several attempts to determine a reliable He−CO interaction potential. In this paper we compare results obtained using two of these. Chuaqui et al. fit a potential (denoted V333) to the original He−CO infrared spectra.[7] Energy levels computed from their potential agree very well with experiment. More recently, Peterson and McBane fit a function (denoted CBS+Corr) to high level ab initio points.[8] Although these were state-of-the-art CCSD(T) calculations, the CBS+Corr potential does not fit the observed spectra as well as the V333 potential. Other ab initio potentials have been obtained using symmetry adapted perturbation theory (SAPT)[26] and density functional theory (DFT),[27] but they also do not fit the observed He−CO spectra as accurately as V333. It is worth noting that both the CBS+Corr and SAPT potentials are 3-dimensional (that is, they explicitly include the dependence on the C−O bond length).

Extensive spectra of the binary complex He−CO have been reported in the infrared and microwave/millimeterwave (MW) regions.[7,28−31] He_N-CO clusters, including He_2-CO, were first studied experimentally in 2003 by means of infrared spectroscopy in the region of the CO fundamental band (∼2143 cm^{-1}).[3] Since then, the infrared study has been extended to larger clusters and to various isotopologues of CO[1,32] and He_N-CO cluster spectra have been obtained in the MW region.[4,5,33] Theoretical simulations of these results using quantum Monte Carlo techniques have been successful in explaining many of

[†] Part of the "Robert W. Field Festschrift".

* Corresponding author. Tucker.Carrington@chem.queensu.ca. Fax: 613-533-6669.

[†] Electronic address: Electronic address: Xiaogang.Wang@umontreal.ca.

[‡] Electronic address: Robert.McKellar@nrc-cnrc.gc.ca.

10.1021/jp904778f CCC: $40.75
Published on Web 10/20/2009

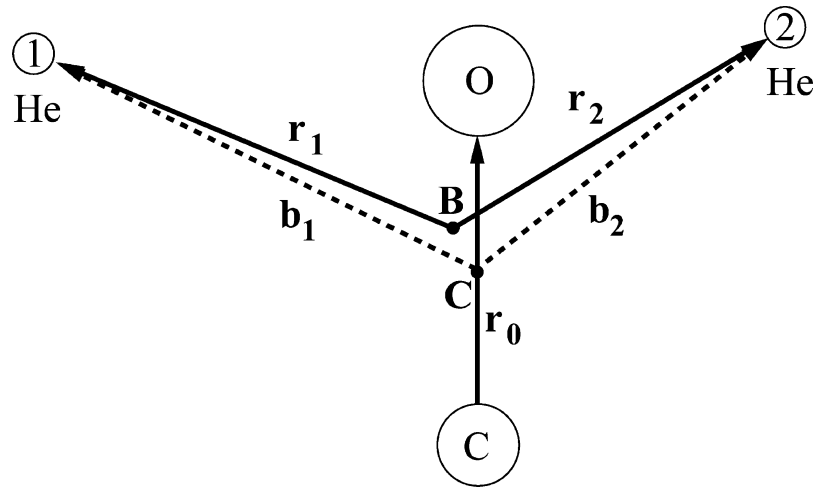

Figure 1. *C* is the center of mass of the dopant. *B* is the canonical point for the Radau vectors. $\mathbf{b_1}$ and $\mathbf{b_2}$ are Jacobi vectors. $\mathbf{r_1}$ and $\mathbf{r_2}$ are Radau vectors. ϕ_2 is a dihedral angle between $\mathbf{r_1}$ and $\mathbf{r_2}$ around $\mathbf{r_0}$. θ_1 (θ_2) are angles between $\mathbf{r_0}$ and $\mathbf{r_1}$ ($\mathbf{r_2}$). The angles are not shown.

the observed trends.[2,34] In addition to these size-resolved spectra of small- and medium-sized He_N−CO clusters, there has also been an infrared study of large ($N > 1000$) helium nanodroplets doped with carbon monoxide.[35]

Turning specifically to spectra of the He_2−CO complex, a total of about 13 transitions have been reported to date: 9 in the infrared region and 4 in the MW region. Many of these could be assigned, at least in an approximate sense, by analogy with the He−CO spectrum. Others were unassigned or, in one case, wrongly assigned. In section IV, below, we show that the present theoretical results support most of the previous empirical assignments but allow the transitions to be understood in much greater detail in terms of the overall energy level structure of He_2−CO. It is also possible to assign a few weaker infrared transitions which were previously overlooked, and to predict positions and intensities for a number of new MW transitions. Before making this comparison with experiment, we first describe the theoretical methods and results in sections II and III.

II. Calculations

A. Kinetic Energy Operator and Basis Functions. We use the approach of ref 6. The kinetic energy operator (KEO) is[6,36,37]

$$T = T_s + T_{b,diag} + T_{b,off} + T_{Cor} \tag{1}$$

with

$$T_s = -\frac{1}{2\mu_1}\frac{\partial^2}{\partial {r_1}^2} - \frac{1}{2\mu_2}\frac{\partial^2}{\partial {r_2}^2}$$

$$T_{b,diag} = -[B_L + B_1(r_1)]\left[\frac{\partial^2}{\partial {\theta_1}^2} + \cot\theta_1\frac{\partial}{\partial\theta_1} - \frac{1}{\sin^2\theta_1}(J_z - l_{2z})^2\right] + [B_L + B_2(r_2)]l_2^2 + B_L[J^2 - 2(J_z - l_{2z})^2 - 2J_z l_{2z}]$$

$$T_{b,off} = B_L[l_{2+}a_1^- + l_{2-}a_1^+]$$

$$T_{Cor} = -B_L[J_+a_1^+ + J_-a_1^- + J_+l_{2+} + J_-l_{2-}] \tag{2}$$

where

$$B_i(r_i) = \frac{1}{2\mu_i r_i^2} \qquad l_{2\pm} = l_{2x} \pm \imath l_{2y}$$

$$J_\pm = J_x \pm \imath J_y \qquad a_1^\pm = \pm\frac{\partial}{\partial\theta_1} - \cot\theta_1(J_z - l_{2z}) \tag{3}$$

The coordinates r_1 and r_2 are the lengths of Radau vectors $\mathbf{r_1}$ and $\mathbf{r_2}$ that are linear combinations of Jacobi (or satellite) vectors, $\mathbf{b_1}$ and $\mathbf{b_2}$, from the He atoms to the center of mass of CO. See Figure 1. $\mathbf{r_0}$ is a vector along CO whose length is fixed. (θ_1, θ_2, ϕ_2) are polyspherical angles determined by three vectors ($\mathbf{r_0}$, $\mathbf{r_1}$, $\mathbf{r_2}$). ($\mathbf{r_1}$, $\mathbf{r_2}$) are also called orthogonalized satellite vectors.[38] $\mu_1 = \mu_2$ is the mass of the He atom. When $\theta_1 = 0$, He atom one is aligned with CO as C−O−He_1. B_L is the rotational constant of the linear dopant CO for the appropriate vibrational state of CO. The l_2 angular momentum operator is defined in terms of the polar angles (θ_2 and ϕ_2) of the Radau vector associated with He atom 2. *J* is the total angular momentum.

We use discrete variable representation (DVR) functions[21,39] for the stretch coordinates and for the bend and rotational coordinates we use the parity adapted rovibrational functions ($\bar{m}_2 = -m_2$ and $\bar{K} = -K$)

$$|u^{JMP}_{l_1 l_2 m_2;K}\rangle = N_{m_2,K}\frac{1}{\sqrt{2}}[|l_1 l_2 m_2;JKM\rangle + (-1)^{J+P}|l_1 l_2 \bar{m}_2;J\bar{K}M\rangle] \tag{4}$$

with

$$N_{m_2,K} = (1 + \delta_{m_2,0}\delta_{K,0})^{-1/2}$$

The ket in this equation is defined by

$$\langle\theta_1,\theta_2,\phi_2;\alpha,\beta,\gamma|l_1 l_2 m_2;JKM\rangle = \sqrt{\frac{2J+1}{8\pi^2}}\Theta_l^{m_1}(\theta_1)\, Y_{l_2}^{m_2}(\theta_2,\phi_2)\, D^{J*}_{MK}(\alpha,\beta,\gamma) \tag{5}$$

with

$$Y_{l_2}^{m_2}(\theta_2,\phi_2) = \frac{1}{\sqrt{2\pi}}\Theta_{l_2}^{m_2}(\theta_2)e^{\imath m_2\phi_2} \qquad m_1 \equiv K - m_2 \tag{6}$$

where $\Theta_l^m(\theta)$ is a normalized associated Legendre function with the $(-1)^m$ Condon−Shortley phase factor. D^J_{MK} is a Wigner function[40] and (α, β, γ) are the Euler angles. For the parity adapted functions, $K \geq 0$ and $P = 0$ and 1 correspond to even and odd parity. If $K = 0$, it is necessary to apply the constraint $m_2 \geq 0$. The combination $m_2 = K = 0$ and $(-1)^{J+P} = -1$ is not allowed. In our calculations l_1, l_2, and m_2 all have the same maximum value. The parity adapted basis makes it possible to calculate even and odd parity levels separately. Within each parity block we use the symmetry adapted Lanczos algorithm[41,42] (SAL) to compute states that are symmetric (*A*) and antisymmetric (*B*) with respect to

TABLE 1: Geometry of the Global He_2CO Minimum on the Potential Made with the $v = 0$ Adiabatic Surface[a]

potential	coordinates	r_0	$r_1 = r_2$	$\theta_1 = \theta_2$	ϕ_2
V333 potential	orthogonalized satellite	2.132	5.8074	59.585	53.43
	satellite	2.132	6.4131	58.68	61.47
CBS+Corr potential	orthogonalized satellite	2.1322	5.8148	71.261	61.11
	satellite	2.1322	6.4218	70.74	55.01

[a] The energy at the minimum is −53.43 (−52.25) cm^{-1} for the V333 (CBS+Corr) potential. Lengths are in bohr and angles are in degrees.

TABLE 2: $J = 0, 1, 2, 3$ Rovibrational Levels (in cm^{-1}) Computed Using the V333 Potential[7] for the $v = 0$ State of CO[a]

A+	B+	A−	B−
	$J = 0$		
0.0000	4.9904	11.3866	4.3703
1.9457	6.6154		7.1782
5.1763	6.9592		
5.8120	7.9153		
7.0800	8.7564		
7.4674			
8.1663			
8.8337			
	$J = 1$		
4.4350	0.7950	0.5143	0.5238
6.0939	3.5805	3.3870	2.3650
	4.5324	4.2488	5.4325
	5.9065	5.5452	5.6500
	6.8197	6.0301	6.2749
		6.4841	
	$J = 2$		
1.2018	1.3707	2.0551	1.8329
1.9481	4.0937	4.6820	5.0278
3.3011	4.8219	5.0730	5.2795
4.9374	6.1747	6.1880	5.6032
5.4426	6.2361		
6.5387			
6.7458			
6.9855			
	$J = 3$		
3.5079	3.1182	2.3296	2.2622
6.1737	3.8089	3.5610	3.2901
6.3080	6.0005	5.2054	4.8550
6.9370	6.3126	5.7020	5.8615
	6.4962	6.2244	6.5073

[a] Levels up to 9 cm^{-1} for $J = 0$ and up to 7 cm^{-1} for $J = 1, 2, 3$ are presented. B+ and B− levels are forbidden. The ZPE is −13.1302 cm^{-1} for the $v = 0$ state.

TABLE 3: Some States Assignable with the Free Rotor Model[a]

J	$(l_0; l_1, l_2)$	sym	zero-order energy	energy	$\langle l_0^2 \rangle$
0	(0; 0, 0)	A−	0.00	0.0000	0.46
0	(0; 1, 0) + (0; 0, 1)	A−	0.50	0.5143	0.48
0	(0; 1, 0) − (0; 0, 1)	B−	0.50	0.5238	0.46
0	(0; 1, 1)	A+	1.00	1.9457	0.38
1	(1; 0, 0)	A−	4.00	4.2487	2.17
1	(1; 1, 0) + (1; 0, 1)	A+	4.50	5.8120	1.56
1	(1; 1, 0) − (1; 0, 1)	B+	4.50	4.9904	2.12
2	(0; 2, 0) + (0; 0, 2)	A+	1.50	1.9480	0.46
2	(0; 2, 0) − (0; 0, 2)	B+	1.50	1.3706	0.48

[a] Energies (in cm^{-1}) are on the He_2CO potential made from the V333 HeCO potential.[7]

exchange of the two He atoms. For more detail see ref 6. A complete product basis function is

$$f_{\alpha_1}(r_1)\, f_{\alpha_2}(r_2)\, u^{JMP}_{l_1 l_2 m_2 K}(\theta_1,\theta_2,\phi_2;\alpha,\beta,\gamma) \qquad (7)$$

where $f_{\alpha_k}(r_k)$ is a DVR function.

B. Computing Rovibrational Energy Levels and Intensities. The SAL algorithm makes it possible to do a single calculation for each parity block that yields both the symmetric and antisymmetric states with respect to permuting the two He atoms: A+ and B+ for even parity, A− and B− for odd parity. For $^4He_2-CO$ only A+ and A− states are physically allowed because of the zero nuclear spin of the ^4He nucleus. Eigenvalues and eigenvectors are obtained by computing matrix−vector products. Similar techniques have been used to compute energy levels of many molecules.[43−46] Kinetic energy matrix elements are given in ref 6. Potential matrix−vector products are evaluated by using quadrature and doing sums sequentially, as explained in ref 6.

To compute intensities, we use standard equations (see ref 6) and assume that the dipole moment is along the CO axis. Specifically, the line strength (S) and intensity (I) for microwave (MW) and infrared (IR) transitions are computed from the wave functions using eqs 28 and 34 of ref 6, respectively. Note that the line strength does not depend on the temperature. The wave functions are obtained from eigenvectors of the Hamiltonian matrix that are computed as described previously.[23,24]

C. Details specific to He_2-CO. We use different rotational constants for $v = 0$ and $v = 1$; v is the quantum number associated with the CO stretch. Following refs 26 and 27, the CO rotational constants are 1.9225125 and 1.9050074 cm^{-1} for $v = 0$ and for $v = 1$.[47] The potential we use for He_2-CO is a sum of two He−CO potentials and a He−He potential. The He−CO potentials of refs 7 and 8 were used. The V333 surface by Chuaqui et al. was obtained by fitting a potential to observed transitions near the fundamental band of CO. The CBS+Corr surface by Peterson and McBane is obtained with state of the art ab initio and extrapolation methods. By computing rovibrational levels from this surface, we assess the accuracy attainable with modern ab initio methods. Note that when using the V333 potential we have the same He−CO potential for both the $v = 0$ and $v = 1$ CO vibrational states, but that we use two different (averaged) CBS+Corr surfaces. The He−He potential of ref 48 was used. The He_2-CO potential is zero when all three of the constituents of the complex are far apart. The orthogonal satellite and satellite coordinates of the equilibrium geometries are given in Table 1. Note that at the He_2-CO minimum, both He−CO and He−He also assume their equilibrium geometries (which would not be true if there were three or more He atoms). The minimum CBS+Corr geometry for He−CO in Table 1 is for the 2D $v = 0$ CBS+Corr surface and is not the same as the minimum geometry given in ref 8 because the latter is for their 3D potential. Compared to the other systems we have studied, He_2-N_2O and He_2-CO_2, the difference between these two sets of coordinates is larger because CO is lighter. The masses are 4.0026u for ^4He and 15.99491u for ^{16}O.

To reduce the spectral range and thereby accelerate the convergence of the Lanczos calculation, it is useful to apply a potential ceiling value.[49] We use a ceiling of 1000 cm^{-1} and have confirmed that low-lying energy levels change by less than

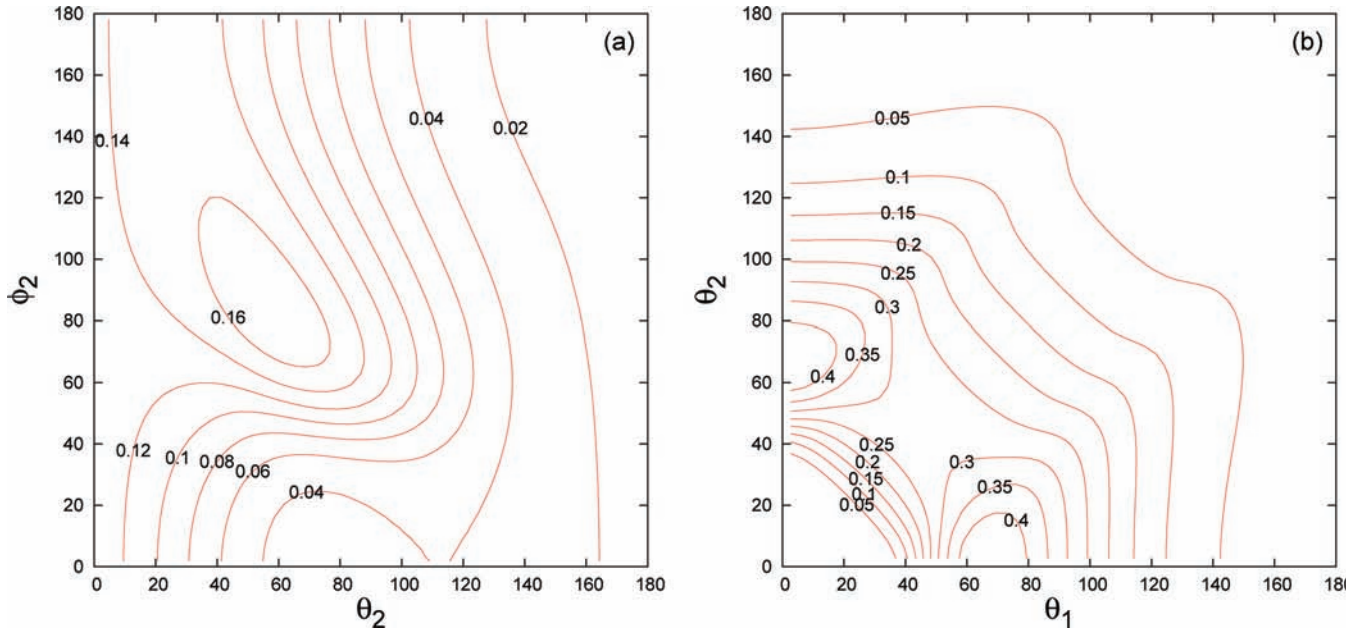

Figure 2. Probability function plots for the ground state with $E = 0.0$ cm^{-1} (A+).

0.001 cm^{-1} when the ceiling is raised to 10000 cm^{-1}. For the angular basis we use $l_{max} = m_{max} = 20$ (the same l_{max} for l_1 and l_2). We use 25 Gauss−Legendre quadrature points for θ_1 and θ_2, and 64 equally spaced points in the range [0, 2π] for ϕ_2. For r_1 and r_2 we use 35 sine DVR functions in the range [3 bohr, 23 bohr].[50,51] Sine DVR is found to be better than potential optimized DVR[52,53] because there is no good choice for a reference potential owing to the fact that r_1 and r_2 are Radau vectors and the helio center (the dopant) is light enough that Radau vectors deviate significantly from the Jacobi vectors. The basis size and the number of quadrature points have been chosen to ensure that the levels we report are converged within 0.001 cm^{-1}. The size of the product basis defined above is 4.1 million for the case of $J = 0$ even parity. The size grows by a factor of $2J + 1$ if $J > 0$.

To compare our computed energy levels directly with experimental results, we calculate IR rovibrational transition wavenumbers from

$$\tilde{\nu} = \tilde{\nu}_0 + E(\upsilon = 1) - E(\upsilon = 0) \quad (8)$$

where $\tilde{\nu}_0 = 2143.221$ cm^{-1} is an experimental band center. $E(\upsilon = 0)$ and $E(\upsilon = 1)$ are calculated wavenumbers measured from the $\upsilon = 0$ and $\upsilon = 1$ ground states.

III. Theoretical Results

In Table 2 we report $\upsilon = 0$ energy levels. Those for $\upsilon = 1$ (not shown here) are very similar, differing only because we use the appropriate B_L values for the $\upsilon = 0$ and $\upsilon = 1$ calculations. This automatically includes part of the effects of the CO vibration on the energy levels. The 2d CBS+Corr surface we use is obtained from their 3d surface by averaging it over a CO wave function; this partially takes into account the CO vibration. This is certainly better than fixing the CO stretch, nonetheless, the V333 potential is more accurate (vide infra). We can compare with the energies obtained using the reptation quantum Monte Carlo (MC) method on the same CBS+Corr potential.[34] Although the MC energies are off (by about 20%), the weights for the R(0) a-type and b-type transitions, 0.28:0.76, agree well with our line strengths (0.20:0.70).

A. Free Rotor Model Assignments. There are two natural zeroth-order models for assigning states of a van der Waals complex like He_2−CO. In both models coupling is neglected so that the Hamiltonian can be separated into pieces and quantum numbers for the pieces used to assign states of the full Hamiltonian. In this assignment discussion we ignore the stretch coordinates because exciting the stretches of He_2−CO causes the complex to dissociate. In the first, body-fixed, model rotation−vibration coupling is neglected and ro-vibrational states are labeled by associating $2J + 1$ rotational states, labeled as J_{K_a,K_c} with each vibrational state (there are only three bending vibrational modes). In the second, space-fixed, model (or free rotor model) one uses as coordinates pairs of spherical polar angles for three vectors. A separable model is obtained by neglecting the potential coupling. We use the orthogonal satellite vectors $\mathbf{r_0}$, $\mathbf{r_1}$, and $\mathbf{r_2}$. One might also use the satellite vectors $\mathbf{r_0}$, $\mathbf{b_1}$, and $\mathbf{b_2}$. The potential is probably more nearly separable in the satellite coordinates, but the corresponding KEO has cross terms that couple coordinates. We choose the orthogonalized satellite vectors because they are the dynamical coordinates used in the calculation. Some of the low-lying He_2−CO states we compute can be assigned using this space-fixed model. The appropriate angular momentum quantum numbers are l_0, for $\mathbf{r_0}$, l_1, for $\mathbf{r_1}$, l_2, for $\mathbf{r_2}$; J, the total angular momentum; and l_{12}, the angular momentum quantum number for the vector sum $\mathbf{l_1} + \mathbf{l_2}$. For some of the low-lying levels we can assign (J; l_0; l_1, l_2) labels, by using the following guidelines. (1) Zeroth-order energies are $B_{CO}l_0(l_0 + 1) + B_{He-CO}l_1(l_1 + 1) + B_{He-CO}l_2(l_2 + 1)$, where $B_{CO} \sim 2$ cm^{-1} and $B_{He-CO} \sim 0.25$ cm^{-1}. (2) The expectation value of $\hat{l}_0^2$, defined in the space-fixed frame, computed with the wave function of a state assigned to l_0, should be close to $l_0(l_0 + 1)$. To determine the expectation value, we must write $\hat{l}_0^2$ in terms of the body-fixed coordinates we use to compute the wave functions. This is done by extracting all the terms in the body-fixed KEO with a B_L coefficient. $\hat{l}_0^2$ expectation values help distinguish between $l_0 = 0$ states and $l_0 \neq 0$ states. (3) The parity must be $(-1)^{l_0+l_1+l_2}$. (4) Transitions between levels with values of l_0 that differ by one should be most intense (these transitions are called b-type transition because the b principal axis is nearly parallel with CO). Space-fixed labels

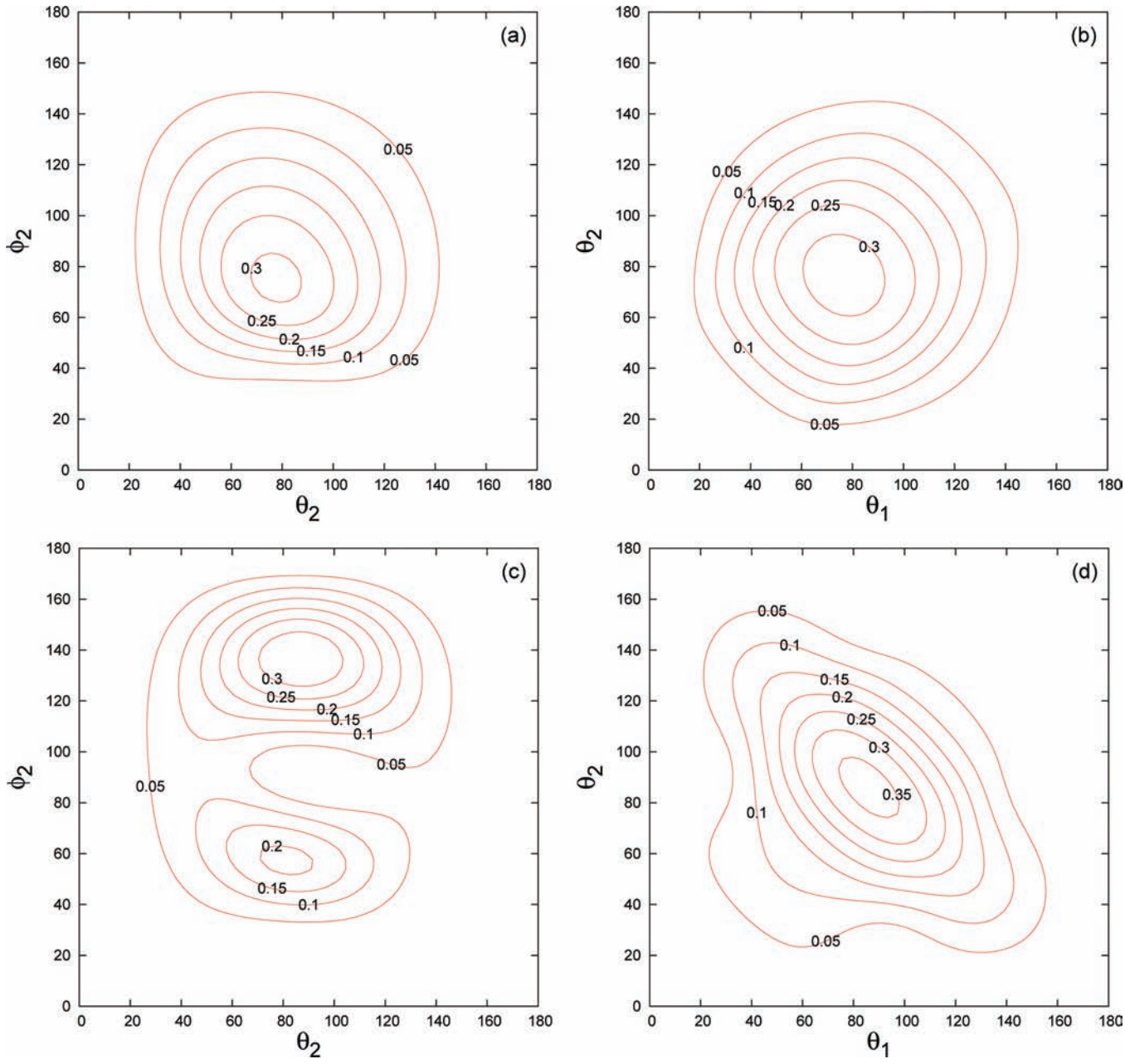

Figure 3. Probability function plots for two torsional states. (a) and (b) are the $\upsilon_t = 1$ torsional state with $E = 4.37$ cm^{-1} (B−). (c) and (d) are the $\upsilon_t = 3$ torsional state with $E = 7.18$ cm^{-1} (B−). The $\upsilon_t = 1$ state appears surprisingly weakly coupled for the three angles examined here.

for $J = 0$ and $J > 0$ states for which they are clearly meaningful are given in Table 3. For example, the levels we have assigned to symmetric and antisymmetric combinations of the (J; l_0; l_1, l_2) = (1; 0; 1, 0) and (1; 0; 0, 1) states have energies very close to $2B_{He-CO}$. For other levels the discrepancies between the zeroth-order energy and the actual energy are larger; e.g., for the A+ level whose assignment is (0; 0; 1, 1), the energy, 1.95 cm^{-1}, is much larger than the zeroth-order energy of 1.0 cm^{-1}. In the last column of Table 3 $l_0 = 0$ states have $\hat{l}_0^2$ expectation values close to 0.5.

B. Characteristics of Some Vibrational States. Two plots of a probability distribution obtained from the ground state wave function, computed on the surface made with the V333 potential, are shown in Figure 2a,b. The probability distribution is obtained by integrating the square of the ground state wave function over the coordinates that are not plotted. It is plotted against (θ_2, ϕ_2) and (θ_1, θ_2) because these coordinates play an important role in assigning and understanding many vibrational states. The ground state has significant amplitude at configurations with one He nearly on top of O. This is not unexpected because the He−CO potential has a small barrier separating the equilibrium geometry from the $\theta = 0$ geometry (that is, C−O−He). The He−C−O barrier is larger ($\theta = 180$) and there seems to be little amplitude with a He atom below C in Figure 1. The wave function peaks near $\phi_2 = 90$ (Figure 2a). On the (θ_1, θ_2) plot, the wave function peaks where one He is near its equilibrium position and the other He is at the O end of CO. The wave function has a broad high plateau near (θ_{1e}, θ_{2e}). The low barrier at $\theta = 0$ exerts a strong influence on the ground state (and many excited states) causing the wave function to delocalize and allowing one He to reside at at the O end of CO.

He_2−CO has bend vibrations similar to the bend of He−CO but it also has a new bending type motion. An interesting vibrational state is the one associated with one excitation of this new mode. Space-fixed labels are not appropriate for this state because its nature is largely determined by the potential.

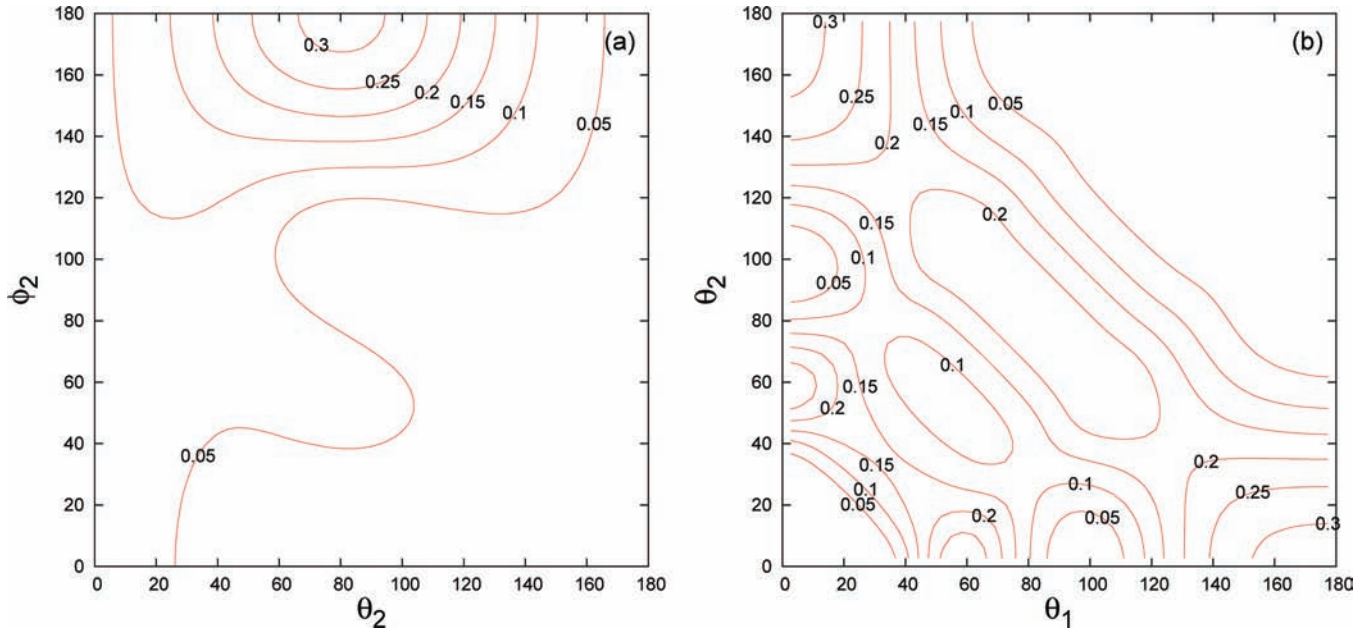

Figure 4. Probability function plots for the first excited vibrational state with $E = 1.95$ cm^{-1} (A+).

For clusters with two He atoms for which the dopant is NNO, OCS, or CO_2, it is appropriate to call this new bend, with B− symmetry, a torsion because it corresponds to movement of the two He around a ring surrounding the dopant. Interestingly the torsion frequency for all these dopants is about 0.5 cm $^{-1}$.[6,9,10] Note that this torsion state and other vibrational states that are not A+ or A− are not physically allowed (for $J = 0$), but still interesting because there are allowed excited rovibrational levels that are associated with forbidden vibrational states. The wave function of the lowest B− state for the CO case is shown in Figure 3a,b. Although its energy ∼4.37 cm^{-1} is much higher than 0.5 cm^{-1} it is clearly a torsion-like state. The higher energy is probably due in part to the weakness of the He−CO interaction. The lowest torsional state has strikingly regular wave functions, which implies that there is little coupling between (θ_2, ϕ_2) and between (θ_1, θ_2). It is not possible to find a state whose wave function has the characteristics expected of a $\upsilon_t = 2$ torsional state. This is probably due to the fact that there are many nearby A+ states (one of them at 1.95 cm^{-1} is discussed in the next paragraph) that couple and distort its character. However, we do find a possible $\upsilon_t = 3$ state (see Figure 3c,d). Its energy is unexpectedly low, 7.18 cm^{-1}. It does not seem to be possible to explain the pattern of the torsional states with a 1d model using a cut through the potential. When we compute energy levels with the He−CO distances, θ_1, and θ_2 fixed, the energy of the $\upsilon_t = 1$ torsion state changes significantly, implying that it is not a simple motion. Stretch−bend coupling seems to be much more important for the CO complex than for the NNO and other complexes.

The torsion is not the only state for which the CO doped cluster differs significantly from other clusters. In other clusters $\upsilon_t = 1$ is the lowest excited vibrational state. In the CO cluster an A+ state at 1.95 cm^{-1} is the lowest. On the (θ_2, ϕ_2) plot (Figure 4a), this state has some amplitude at $\phi_2 = 180$. On the (θ_1, θ_2) plot (Figure 4b), there are peaks at geometries with one He above the O atom (see Figure 1) and the other He at equilibrium (a feature shared by the first, third, and fourth A+ states with $E = 0$ cm^{-1}, $E = 5.18$ cm^{-1}, and $E = 5.81$ cm^{-1}); there is also amplitude at a linear configuration with one He on top of O and the other He below C (a feature shared by the third A+ state with $E = 5.18$ cm^{-1}). This indicates strong coupling between these A+ states. The motion that corresponds to the 1.95 cm^{-1} state is difficult to characterize. The wave function of the third A+ state with $E = 5.18$ cm^{-1} is similar to the wave function of the $E = 1.95$ cm^{-1} state.

In the He−CO complex the $J = 0$ state at 5.39 cm^{-1} is assigned to the bend vibration and given space-fixed quantum numbers $l_0 = 1$; $l_1 = 1$. In He_2−CO one expects two bend vibrations that are symmetric and antisymmetric combinations of He−CO bends, and we assign the A+ state at 5.81 cm^{-1} and the B+ state at 4.99 cm^{-1} to these bends. In terms of space-fixed labels they are combinations of (J; l_0; l_1, l_2) = (1; 0; 1, 0) and (1; 0; 0, 1) states. Probability distributions for these two states are shown in Figure 5a,b for the A+ state and Figure 5c,d for the B+ state. On the (θ_1, θ_2) plot, the symmetric bend has 4 peaks. At each of the 4 peaks, the θ angle of one of the He atoms is near its equilibrium value and the other He atom is near either the O or the C end of CO. There is little amplitude with both He atoms on the ring. The antisymmetric bend state has only 2 peaks on the (θ_1, θ_2) plot. At both peaks, one He is on the ring, and the other He is near the O end of CO. There is almost no amplitude where both He atoms are on the ring. Therefore, the symmetric He−CO bend states is more delocalized than the antisymmetric states. This is in accord with the fact that stronger couplings are observed in the A+ than in the B+ block.

In many lower states, including the ground state, one He atom is on the ring and the other He atom is near one of the ends of CO. At higher energy, it is expected that in some states the He atoms will sample both ends of CO, and that there will therefore be significant amplitude at linear structures. (θ_1, θ_2) plots of an A+ state with $E = 5.18$ cm^{-1} and a B+ state with $E = 6.62$ cm^{-1} are shown in Figure 6a,b. The two He atoms are completely localized at the ends of CO in the B+ state, whereas the A+ state also has amplitude in nonlinear geometries. Note that if the molecule is linear, the two θ coordinates would be 0 or 180 in both Radau and Jacobi coordinates.

C. Comparison of Theory and Experiment. Spectra showing most of the observed He_2−CO infrared transitions are shown in Figure 7. These were obtained using a tunable diode laser to probe a pulsed supersonic jet expansion from a slit-shaped

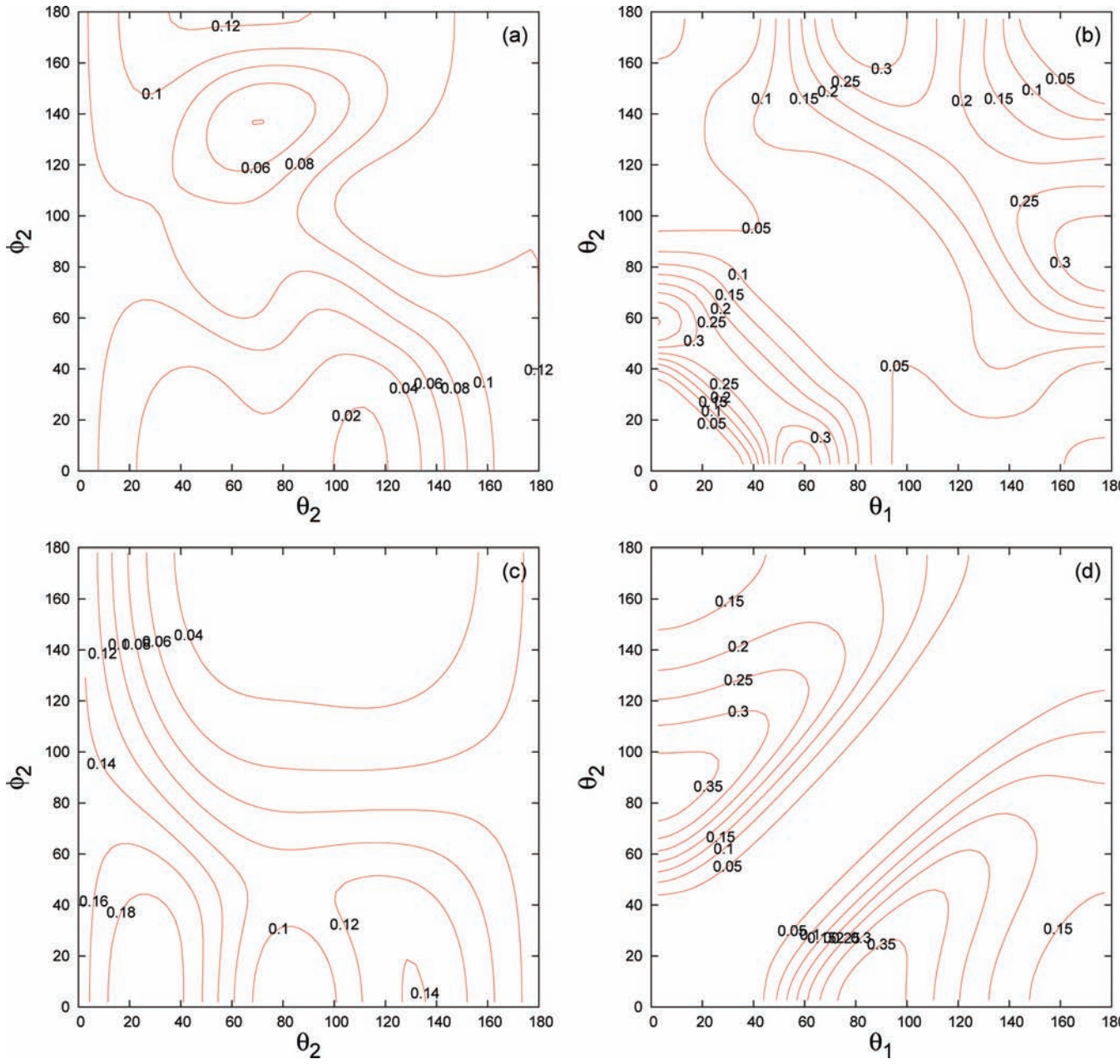

Figure 5. Probability function plots for θ bend states. (a) and (b) are the symmetric bend state with $E = 5.81$ cm^{-1} (A+). (c) and (d) are the antisymmetric bend state with $E = 4.99$ cm^{-1} (B+).

nozzle, as described previously.[3,32] Experimental conditions were chosen to favor the formation of He_2-CO, but there are still transitions present due to CO itself, He−CO, He_3-CO, etc. These are labeled with the numbers (in circles) representing N, the number of He atoms in the He_N-CO cluster, and with the letter "d" denoting transitions assigned to the CO dimer. As noted above, transitions of He_N −CO clusters may be characterized as a- or b-type, corresponding to $\Delta l_0 = 0$ or 1 (where l_0 is the CO angular momentum quantum number). The lower panel in Figure 7 covers the a-type region, and the upper panel covers the b-type region where (for smaller clusters like He_2-CO) the transitions are much stronger. The extremely strong line labeled "0" in the upper panel is the R(0) transition of the CO monomer.

Calculated line positions and intensities for He_2-CO are given in Table 4 for the infrared region and Table 5 for the MW region. Note that only A+ and A− states are physically allowed by nuclear spin statistics for $^4He_2-CO$. The line intensities (denoted by I) are obtained from the line strength factors (denoted by S) by multiplying by temperature dependent factors and the transition frequency, and then normalizing to "the fundamental" lowest 0e → 1o transition. (See eqs 28 and 34 of ref 6.) The effective temperature is chosen to be 0.5 K, which is roughly characteristic of the supersonic jet expansion conditions in which these spectra are observed.

Because the He−CO potentials we use are 2D, we need (see eq 8) the vibrational band center to compute infrared line positions. For both the V333 and the CBS-Corr calculations we use an empirical value, $\tilde{\nu}_0(He_2CO) = 2143.221$ cm^{-1}, which is obtained by taking the midpoint between $P(1)$ (2142.705 cm^{-1}) and R(0) (2143.7376 cm^{-1}). For calculations done with the CBS-Corr potentials we can compute the band center from

$$\tilde{\nu}_0(He_2CO) = \tilde{\nu}_0(CO) + E^{zpe}_{v=1} - E^{zpe}_{v=1} \qquad (9)$$

where $E^{zpe}_{v=0}$ and $E^{zpe}_{v=1}$ are zero-point energies (zpe) obtained on the adiabatic $v = 0$ and $v = 1$ surfaces, respectively, measured

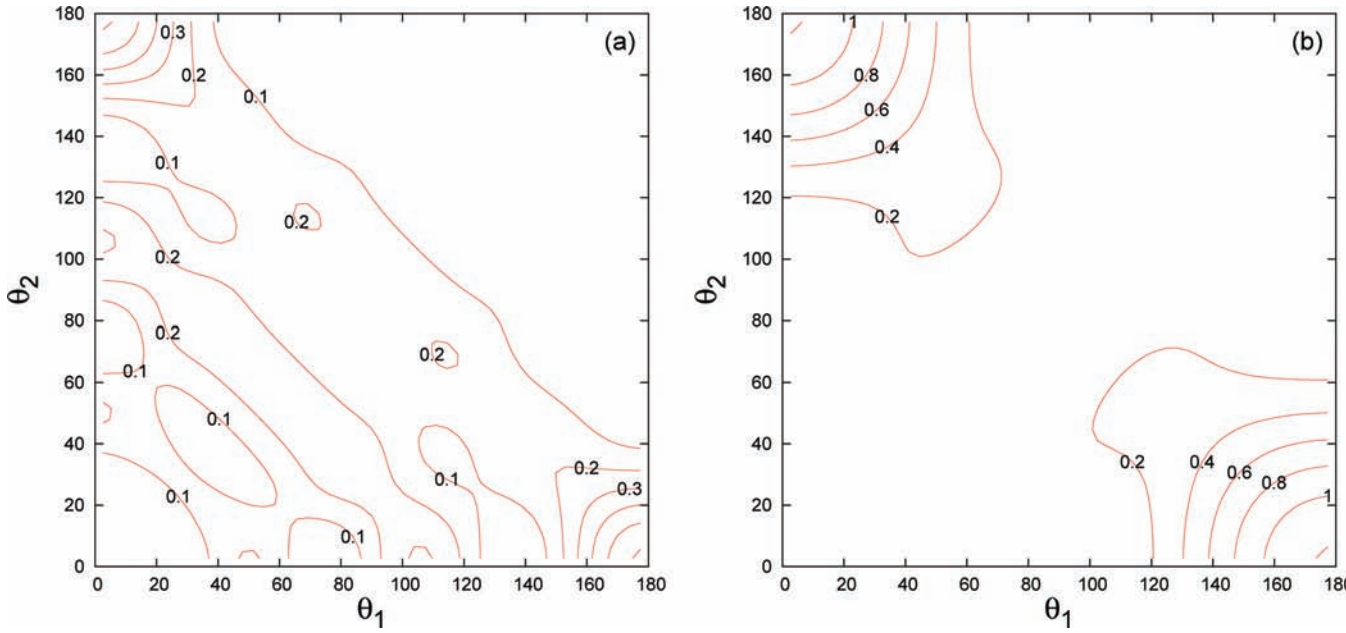

Figure 6. Probability function plots for linear states. (a) is a linear state with $E = 5.18$ cm^{-1} (A+). (b) is a linear state with $E = 6.62$ cm^{-1} (B+). The two He atoms are almost completely localized on the ends of CO for state (b).

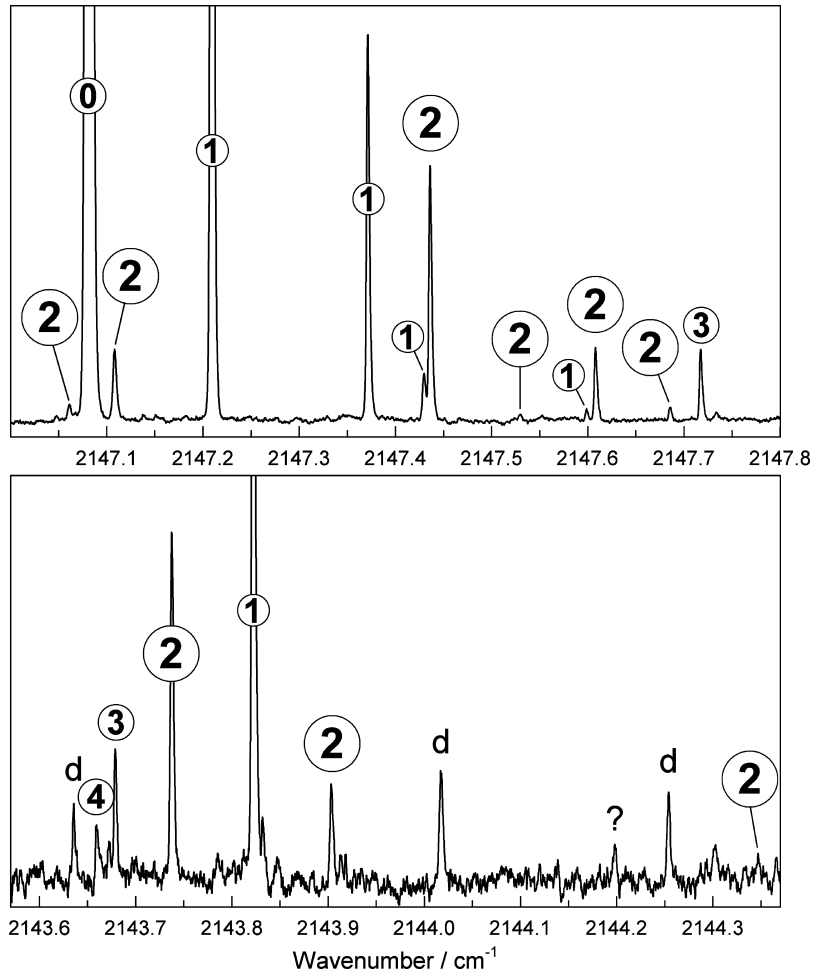

Figure 7. Spectra showing transitions of He_N−CO clusters. The numbers in circles represent N, the number of helium atoms in the cluster responsible for the indicated transition. Transitions due to the CO dimer are indicated by "d", and a mystery transition (originally but mistakenly assigned to He_2−CO) is indicated by "?".

relative to the dissociation asymptote. The band center that we find in this fashion is $\tilde{\nu}_0(He_2CO) = 2143.2222$ cm^{-1}, which is very close to the empirical value. From this band center, we obtain the vibrational band center shift, $E_{shift} = \tilde{\nu}_0(He_2CO) - \tilde{\nu}_0(CO)$, relative to the free CO band center and compare it to the observed shift. See Table 6. The agreement is very good.

TABLE 4: Calculated and Observed Transitions in the Infrared Spectrum of He_2-CO (in cm^{-1}) with Intensities >0.1[a]

$J, P, E(v = 0)$	$J, P, E(v = 1)$	cal	obs	obs − calc	obs − calc[b]	S	I
1o 0.5143	0e 0.0000	2142.7067	2142.705	−0.0017	−0.0013	0.20	0.23
0e 0.0000	1o 0.5140	2143.7350	2143.7376	0.0026	0.0027	0.20	1.00
1o 0.5143	2e 1.2017	2143.9085	2143.903	−0.0054	0.0023	0.64	0.71
2e 1.2018	3o 2.3291	2144.3483	2144.348	0.0003	0.0040	1.60	0.25
1o 0.5143	2e 1.9482	2144.6549	2144.646	0.0089	−0.0085	0.19	0.22
0e 0.0000	1o 3.3857	2146.6067				0.02	0.11
2e 1.2018	2o 5.0453	2147.0645	2147.062	−0.0025	0.0312	1.55	0.24
1o 0.5143	1e 4.4029	2147.1097	2147.109	−0.0006	0.0308	0.57	0.63
0e 0.0000	1o 4.2189	2147.4399	2147.4362	−0.0037	0.0289	0.70	3.44
2e 1.2018	1o 5.5168	2147.5360	2147.530	−0.0060	0.0257	0.72	0.11
1o 0.5143	2e 4.9086	2147.6154	2147.608	−0.0073	0.0279	2.19	2.46
2e 1.2018	3o 5.6760	2147.6952	2147.685	−0.0102	0.0214	4.15	0.64
1o 0.5143	2e 5.4398	2148.1465				0.14	0.16
1o 0.5143	0e 5.7929	2148.4997				0.13	0.14

[a] All calculated values except those in the sixth column are computed with the V333 potential..[7] [b] This calculation is with the CBS+Corr potential.[8]

TABLE 5: Calculated and Observed MW Transitions of He_2-CO (in cm^{-1}) with Intensities >0.8[a]

J, P, E (lower)	J, P, E (upper)	cal	obs	obs − calc	obs − calc[b]	S	I
0e 0.0000	1o 0.5143	0.5143	0.5168	0.0025	0.0021	0.20	1.00
1o 0.5143	2e 1.2018	0.6875				0.63	1.06
0e 0.0000	1o 3.3870	3.3870				0.02	0.90
2e 1.2018	2o 5.0730	3.8712				1.58	2.39
1o 0.5143	1e 4.4350	3.9208	3.9165	−0.0042	0.0281	0.57	6.30
0e 0.0000	1o 4.2488	4.2488	4.2441	−0.0047	0.0270	0.70	37.06
2e 1.9481	3o 6.2244	4.2763				4.65	0.91
2e 1.2018	1o 5.5452	4.3434				0.72	1.23
1o 0.5143	2e 4.9374	4.4232	4.4153	−0.0078	0.0262	2.18	27.37
2e 1.2018	3o 5.7020	4.5002				4.20	7.43
1o 0.5143	2e 5.4426	4.9283				0.16	2.21
2e 1.2018	3o 6.2244	5.0226				0.42	0.82
1o 0.5143	0e 5.8120	5.2978				0.13	1.95
0e 0.0000	1o 6.4841	6.4841				0.02	1.36
0e 0.0000	1o 7.1487	7.1487				0.01	1.07

[a] All calculated values except those in the sixth column are computed with the V333 potential. [b] This calculation is with the CBS+Corr potential.[8]

TABLE 6: CO Stretch Vibrational Band Center Shifts Computed on the CBS-Corr Potential (in cm^{-1})[a]

molecule	$E^{zpe}_{v=0}$	$E^{zpe}_{v=1}$	E^{comp}_{shift}	E^{obs}_{shift}
He−CO	−6.43081	−6.45524	−0.0244	−0.0249[b]
He_2-CO	−13.1302	−13.1792	−0.0490	−0.0492[c]

[a] The free CO vibrational vibrational band center is 2143.2712 cm^{-1}. $E^{comp}_{shift} = E^{zpe}_{v=1} - E^{zpe}_{v=0}$. [b] Refrerence 29. [c] This work.

The calculated line positions from the V333 potential (third column of Table 4) agree well with the observed values (fourth column). Reliable experimental intensities are not available for a number of reasons, but in a qualitative sense there is also good intensity agreement between observation and theory (the effective rotational temperature in the spectra of Figure 7 is evidently somewhat lower than 0.5 K). The three strongest lines due to He_2-CO were corrrectly assigned in ref 3 as b-type R(0), b-type R(1), and a-type R(1) transitions (2147.436, 2147.608, and 2143.738 cm^{-1}, respectively), as were the b-type Q(1) and Q(2) transitions at 2147.109 and 2147.062 cm^{-1}. However, the present calculations show that the original (ref 3) assignment of the a-type R(1) transition was incorrect, and that the true assignment should be to a line at 2143.903 cm^{-1}. The latter had been recognized as being due to He_2-CO, but it was left unassigned because (based on a simple rigid-rotor picture) its position seemed wrong for R(1). The line mistakenly assigned as R(1) at 2144.198 cm^{-1}, indicated by "?" in Figure 4, is evidently not due to He_2-CO. We speculate that it might be a weak transition of He_3-CO. The present calculations allow us to assign three additional lines to He_2-CO at 2144.348, 2144.646, and 2147.530 cm^{-1} (see Figure 4 and Table 4). These lines are quite weak, making it difficult to establish their assignment to He_2-CO on experimental grounds (i.e., dependence of the spectrum on the supersonic jet backing pressure). Thus they are a bit less certain than the other transitions in Table 4, but we are still confident, due to their good agreement with the calculated positions and intensities.

There are four observed lines of He_2-CO available in the literature for the comparison of theory and experiment in the MW region, namely a-type R(0) and b-type Q(1), R(0), and R(1) transitions at 15492.5636, 117414.357, 127234.352, and 132368.279 MHz, respectively.[4,5,33] As shown in Table 5, these agree well with the theoretical values based on the V333 potential. Indeed, the patterns of residuals (obs − calc) are rather similar for the analogous transitions in Tables 4 and 5. It is clear from Table 5 that there are a number of additional MW transitions that should be observable, though there will still be a significant search problem since the precision of MW spectroscopy is much higher than the accuracy of our calculations. For example, using results from Table 5, but with estimated corrections based on the residuals for the observed MW and infrared lines, we might expect the following approximate positions for the a-type R(1), b-type Q(2) and b-type R(2) transitions: 20450, 115905, and 134610 MHz. See the computed stick MW spectrum, Figure 8.

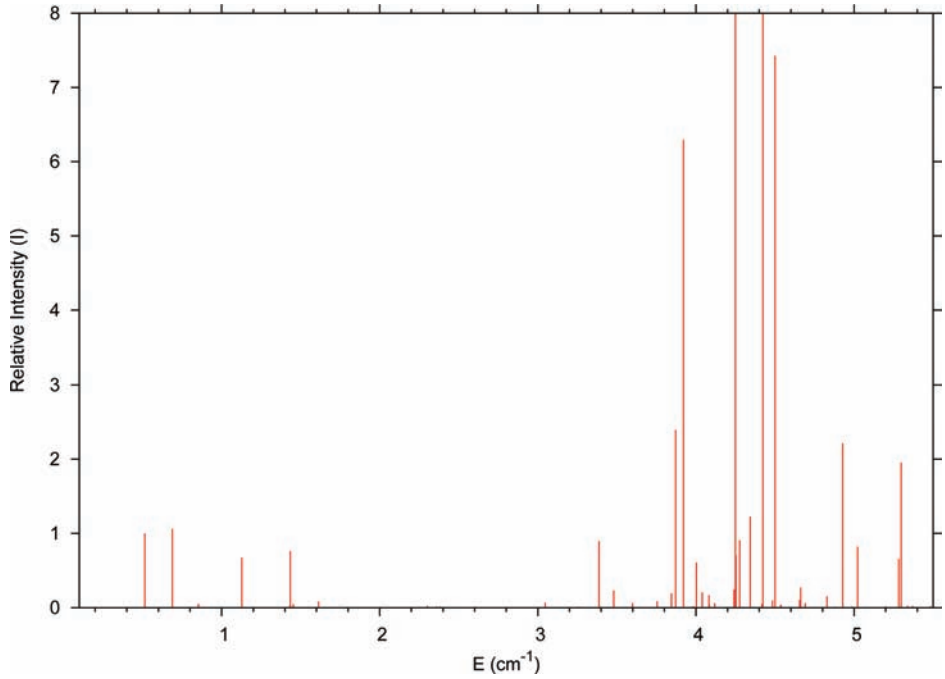

Figure 8. Calculated ($T = 0.5$K) microwave spectra of He_2-CO. The intensity of the R(0) transition is 1. The scale is chosen to reveal weak transitions and therefore strong lines are beyond the range of the figure.

TABLE 7: Test of Different Potentials on Two Representative Levels (in cm^{-1})

		cal − obs		
	obs	V333	CBS+Corr	SAPT
R(0) a-type, He−CO	0.5763	0.0003[a]	−0.0022[b]	0.0054[c]
R(0) a-type, He_2−CO	0.5168	−0.0025[a]	−0.0021[a]	
R(0) b-type, He−CO	3.9954	0.0012[a]	−0.0158[b]	0.0221[c]
R(0) b-type, He_2−CO	3.9165	0.0042[a]	−0.0281[a]	

[a] This work. [b] Reference 8. [c] Reference 26.

In column 6 of Tables 4 and 5, we also list the residuals obtained using the CBS+Corr potential. These are not as good as those from the V333 potential, but they are still consistently within 0.03 cm^{-1} of the experimental line positions. In particular, the CBS+Corr results have consistently larger residuals for the higher energy levels corresponding to rotational excitation of CO, those involved in the b-type transitions. Interestingly, a similar pattern of errors is also found in the He−CO spectra.[31,32] Using the SAPT ab initio potential, the levels with $l_0 = j_{CO} = 1$ are also poorly calculated. The error patterns of the three potentials, V333, CBS+Corr, and SAPT, for the a- and b-type R(0) transitions of He−CO and He_2−CO are shown in Table 7.

IV. Conclusion

Doped helium clusters have been studied intensely in recent years, and these results have helped to develop a better understanding of how superfluid effects depend on cluster size. A thorough understanding of smaller helium clusters facilitates the analysis of larger ones. The spectroscopy of the smaller clusters is also interesting by itself. One conclusion that is certainly relevant for small and probably for large clusters is the high quality of the potential obtained by adding two-body interactions. It is remarkable that one can obtain such good agreement with experiment without including all three-body interactions. To analyze the spectra, one must account for the interaction of many large amplitude vibrations, for which perturbative approaches are insufficient. This is particularly true if the dopant is CO because in this case coupling is especially important. Several other complexes with two helium atoms and a linear dopant have been studied. For the other complexes a model with the helium atoms on a ring encircling the dopant enables one to understand the structure of the spectrum. This is not the case for the CO complexes. The frequency of the torsion is much larger if the dopant is CO. The CO complex differs from the others in part because the CO−He interaction is weak. The weakness of the CO−He interaction increases the effect of coupling to bend coordinates. The CO dopant is sigificantly shorter than triatomic linear dopants and this makes it easier for one or two He atoms to localize at the ends of the dopant.

For He−CO, the energy level structure is simple and it is straightforward to label levels using either a body- or space-fixed system. For He_2−CO a similar space-fixed model is still helpful but not as good. In the CO cluster, rotation of the He atoms around the dopant and rotation of the dopant itself are free enough that a space fixed model is a good starting point. The motion is floppy enough that the traditional rigid-body type approach is poor. Many of the levels are very difficult to assign. However, even when it is not possible to assign computed levels, they can be used to help identify and assign experimental lines. The V333 potential,[7] obtained by fitting to the He−CO spetra, give more accurate He_2−CO energy levels than the state-of-the-art ab initio CBS+Corr potential.[8] On the other hand, the

vibrational band center shift computed on the CBS+Corr potential agrees very well with the experimental result.

If the structure of a linear dopant molecule is fixed, it is now not difficult to compute ro-vibrational spectra for He_2−dopant complexes. Because there are only five vibrational coordinates, converged results can be obtained from a simple (but large) product basis. The spherical harmonic basis functions we use are ideal for treating complexes with large amplitude bend vibrations. To compute spectra for complexes with three He atoms, it would be necessary to use more sophisticated basis functions,[54,55] but such calculations should now be possible.

Acknowledgment. This work has been supported by the Natural Sciences and Engineering Research Council of Canada and the Canada Research Chairs Program. Calculations were done on a computer of the Réseau québécois de calcul de haute performance (RQCHP).

References and Notes

(1) McKellar, A. R. W. *J. Chem. Phys.* **2006**, *125*, 164328.
(2) Cazzato, P.; Paolini, S.; Moroni, S.; Baroni, S. *J. Chem. Phys.* **2004**, *120*, 9071.
(3) Tang, J.; McKellar, A. R. W. *J. Chem. Phys.* **2003**, *119*, 754.
(4) Dumesh, B. S.; Surin, L. A. *Physics - Uspekhi* **2006**, *49*, 1113.
(5) Surin, L. A.; Potapov, A. V.; Dumesh, B. S.; Schlemmer, S.; Xu, Y.; Raston, P. L.; Jaeger, W. *Phys. Rev. Lett.* **2008**, *101*, 233401.
(6) Wang, X.-G.; Carrington, T., Jr.; Tang, J.; McKellar, A. R. W. *J. Chem. Phys.* **2005**, *123*, 034301.
(7) Chuaqui, C. E.; Le Roy, R. J.; McKellar, A. R. W. *J. Chem. Phys.* **1994**, *101*, 39.
(8) Peterson, K. A.; McBane, G. C. *J. Chem. Phys.* **2005**, *123*, 084314.
(9) Tang, J. McKellar, A. R. W. Wang X.-G. Carrington, T., Jr. *Can. J. Phys.* **2009**, *87*, 417−423.
(10) Wang, X.-G. Carrington, T., Jr., Tang, J. McKellar A. R. W. Unpublished results.
(11) Paesani, F.; Viel, A.; Gianturco, F. A.; Whaley, K. B. *Phys. Rev. Lett.* **2003**, *90*, 073401.
(12) Moroni, S.; Sarsa, A.; Fantoni, S.; Schmidt, K. E.; Baroni, S. *Phys. Rev. Lett.* **2003**, *90*, 143401.
(13) Moroni, S.; Blinov, N.; Roy, P.-N. *J. Chem. Phys.* **2004**, *121*, 3577.
(14) Li, H.; Blinov, N.; Roy, P.-N.; Le Roy, R. J. *J. Chem. Phys.* **2009**, *130*, 144305.
(15) Bačić, Z.; Kennedy-Mandziuk, M.; Moskowitz, J. W.; Schmidt, K. E. *J. Chem. Phys.* **1992**, *97*, 6472.
(16) Hernández, M. I.; Halberstadt, N.; Sands, W. D.; Janda, K. C. *J. Chem. Phys.* **2000**, *113*, 7252.
(17) Bramley, M. J.; Tromp, J. W.; Carrington, T., Jr.; Corey, G. C. *J. Chem. Phys.* **1994**, *100*, 6175.
(18) Chen, R.; Ma, G.; Guo, H. *J. Chem. Phys.* **2001**, *114*, 4763.
(19) Carrington, T., Jr. In *Encyclopedia of Computational Chemistry*; Schleyer, P. v. R., Ed.; Wiley: New York, 1998; Vol. 5.
(20) Bowman, J.; Carrington, T., Jr.; Meyer, H.-D. *Mol. Phys.* **2008**, *106*, 2145.
(21) Light, J. C.; Carrington, T., Jr. *Adv. Chem. Phys.* **2000**, *114*, 263.
(22) Wang, X.-G.; Carrington, T., Jr. *J. Chem. Phys.* **2001**, *115*, 9781.
(23) Wang, X.-G.; Carrington, T., Jr. *J. Chem. Phys.* **2003**, *119*, 101.
(24) Wang, X.-G.; Carrington, T., Jr. *J. Chem. Phys.* **2003**, *118*, 6946.
(25) Wang, X.-G.; Carrington, T., Jr. *J. Chem. Phys.* **2002**, *117*, 6923.
(26) Heijmen, T. G. A.; Moszynski, R.; Wormer, P. E. S.; van der Avoird, A. *J. Chem. Phys.* **1997**, *107*, 9921.
(27) Gianturco, F. A.; Paesani, F. *Mol. Phys.* **2001**, *99*, 689.
(28) Chan, M.-C.; McKellar, A. R. W. *J. Chem. Phys.* **1996**, *105*, 7910.
(29) McKellar, A. R. W.; Xu, Y.; Jager, W.; Bissonnette, C. *J. Chem. Phys.* **1999**, *110*, 10766.
(30) Surin, L. A.; Roth, D. A.; Pak, I.; Dumesh, B. S.; Lewen, F.; Winnewisser, G. *J. Chem. Phys.* **2000112**, 4064. Erratum, *J. Chem. Phys.* 2000, 112, 9190.
(31) Potapov, A. V.; Surin, L. A.; Panfilov, V. A.; Dumesh, B. S. *Opt. Spectrosc.* **2009**, *106*, 183.
(32) McKellar, A. R. W. *J. Chem. Phys.* **2004**, *121*, 6868.
(33) Surin, L.; Winnewisser, G.; Potapov, A.; Dumesh, B. *Proceedings of the 19th Colloquium on High-Resolution Spectroscopy*, Salamanca; 2005; p 172.
(34) Škrbić, T.; Moroni, S.; Baroni, S. *J. Phys. Chem. A* **2007**, *111*, 7640.
(35) von Haeften, K.; Rudolph, S.; Simanovski, I.; Havenith, M.; Zillich, R. E.; Whaley, K. B. *Phys. Rev. B* **2006**, *73*, 054502.
(36) Chapuisat, X.; Iung, C. *Phys. Rev. A* **1992**, *45*, 6217.
(37) Gatti, F.; Iung, C.; Menou, M.; et al. *J. Chem. Phys.* **1998**, *108*, 8804.
(38) Mladenovic, M. *J. Chem. Phys.* **2000**, *112*, 1070.
(39) Light, J. C.; Hamilton, I. P.; Lill, J. V. *J. Chem. Phys.* **1985**, *82*, 1400.
(40) Zare, R. N. *Angular Momentum*; Wiley: New York, 1988.
(41) Wang, X.-G.; Carrington, T., Jr. *J. Chem. Phys.* **2001**, *114*, 1473.
(42) Chen, R.; Guo, H. *J. Chem. Phys.* **2001**, *114*, 1467.
(43) Bramley, M. J.; Carrington, T., Jr. *J. Chem. Phys.* **1994**, *101*, 8494.
(44) Light, J. C.; Carrington, T., Jr. *Adv. Chem. Phys.* **2000**, *114*, 263.
(45) Carrington, T., Jr. *Encyclopedia of Computational Chemistry*; Schleyer, P. v. R., Editor in Chief; John Wiley & Sons, 1998; Vol. 5.
(46) Chen, R.; Guo, H. *J. Chem. Phys.* **1998**, *108*, 6068.
(47) Mantz, A. W.; Watson, J. K. G.; Rao, K. N.; Albritton, D. L.; Schmeltekopf, A. L.; Zare, R. N. *J. Mol. Spectrosc.* **1971**, *39*, 180.
(48) Aziz, R. A.; McCourt, F. R. W.; Wong, C. C. K. *Mol. Phys.* **1987**, *61*, 1487.
(49) Bramley, M. J.; Tromp, J. W.; Carrington, T., Jr.; Corey, G. C. *J. Chem. Phys.* **1994**, *100*, 6175.
(50) Leforestier, C. *J. Chem. Phys.* **1991**, *94*, 6388.
(51) Colbert, D. T.; Miller, W. H. *J. Chem. Phys.* **1992**, *96*, 1982.
(52) Wei, H.; Carrington, T., Jr. *J. Chem. Phys.* **1992**, *97*, 3029.
(53) Echave, J.; Clary, D. C. *Chem. Phys. Lett.* **1992**, *190*, 225.
(54) Wang, X.-G.; Carrington, T., Jr. *J. Chem. Phys.* **2002**, *117*, 6923.
(55) Wang, X.-G.; Carrington, T., Jr. *J. Chem. Phys.* **2003**, *119*, 101.

JP904778F